

# Biphonons in the Klein-Gordon lattices

Laurent Proville

*Service de Recherches de Métallurgie Physique,  
CEA/DEN/DMN Saclay 91191-Gif-sur-Yvette Cedex, France*

(Dated: December 2, 2024)

## Abstract

A numerical approach is proposed for studying the optical modes in the quantum lattices where the atomic displacements yield a non-quadratic contribution to the lattice energy. The study is focussed on the pairing of the phonon states due to the non-quadratic energy terms. When these terms are significant a biphonon state occurs<sup>1</sup> and the biphonon spectral branch splits from the 2 phonon band by the opening of a gap. The width of the gap reveals the magnitude of the non-quadratic energy. For the purely quadratic lattice the biphonon gap vanishes and the biphonon dissociates into a pair of free phonons. When the non-quadratic energy contribution is not negligible but is weaker than the band width of the phonon states, then a pseudogap is proved to open at the edge of the lattice Brillouin zone while at the center the biphonon gap vanishes. The pseudogap is found to be a consistent feature of the lattices where the non-quadratic contribution is moderate. Considering the space correlation properties of the biphonon, in the lattices where a biphonon gap opens the biphonon states are then proved to exhibit a finite length scale for some specific forms of the non-quadratic energy that are determined. The results are extended to the multi-phonon bound states and the quantum breather modes<sup>2</sup> are identified.

PACS numbers: 63.20.Ry, 03.65.Ge, 11.10.Lm, 63.20.Dj

## I. INTRODUCTION

In condensed matter as well as for a single molecule, the proximity of the atoms involves a coupling between the atomic displacements and consequently some elementary excitations, namely the phonons. At the atomic scale, some non-quadratic terms appears formally in the development of the effective interactions between the neighboring atoms with respect to their displacements. Those terms usually refer to the nonlinearity because they yield some atomic forces that are not proportional to the displacements. The nonlinear contribution have no effect over the phonon energy which could be distinguished from a rescaling of the quadratic terms so no evidence for the nonlinear behavior comes from the phonon analysis. The scope must be put on the higher energy excitations for detecting the signature of the nonlinearity.

The non-quadratic energy of crystals have been extensively studied by V.M. Agranovich<sup>1</sup> who proposed a qualitative approach where an effective interaction between the phonon quasi-particles yields a pairing of the phonon states. The concepts of the phonon bound states and more specifically of the biphonon were of a great help for interpreting some experiments where anharmonic modes were measured (see Ref. 3 for infrared, Ref. 4 for neutron spectra and references therein). In the early seventies<sup>5</sup>, the phonon bound states have indeed been identified in the infrared analysis of the bulk crystals as for the  $N_2O$  or the  $CO_2$ . For such molecular crystals, the intra-molecular bond involves a strong non-quadratic contribution and the pairing of the stretching modes is revealed by some anharmonic resonances that are isolated in the infrared spectrum.

The debate about the spectral branch  $\Delta'_2(\text{LO})$  of the diamond (see Refs. 6,7 for the different points of view) showed that the interpretations of the experimental spectrum may diverge when the magnitude of the non-quadratic terms is not sufficient for yielding some isolated resonances in the overtone regions. In truth, when the nonlinearity is not specially strong every term of the inter-atomic potential must be treated on equal footing. In particular, the energy contributions that do not conserve any ad'hoc quanta number must be taken into account. The work of A. R. Bishop *and al.*<sup>2</sup> confirms the existence of the phonon bound states in a model which does not require the commutation of the atomic network Hamiltonian with a quanta number operator. Furthermore, the existence of some phonon bound states with a particle-like energy band was enhanced for certain model parameters. The so-called

quantum breathers (see also Refs. 8,9,10,11) are characterized by a finite correlation length and they have some classical mechanic counterparts that are the discrete breather solutions in the nonlinear classical lattices<sup>12,13</sup>. Nonetheless, the numerical approach in Ref. 2 requires a huge computing cost so the maximum size of the Hamiltonian network was limited to a one-dimensional chain of 8 unit cells. Moreover, the numerical simulations were restricted to the parameter region where the non-quadratic part of the lattice energy is modelled by a quartic onsite potential, i.e., the well-known discrete  $\phi^4$  model.

In the present work, a numerical method is introduced for studying the energy spectrum of a d-dimensional quantum lattice with a generic nonlinearity. Starting from the exact calculation of the eigenstates of the Hamiltonian network where no interaction couples the displacement of the atoms at site  $i$ , the low energy states are used to construct a set of Bloch waves upon which is expanded the whole Hamiltonian including the coupling between the displacements of the first atom neighbors in a realistic manner, i.e., with no ad'hoc quanta conservation. The Shrödinger equation is then approximately solved with an error which shrinks to zero by increasing the energy cutoff over the eigenstates of the uncoupled network. The advantage of this method is twofold. First it is not parameter-dependant of the nonlinearity. Second, thanks to the Bloch wave formulation, the maximum size of the lattices that are studied is large enough for approaching the infinite system features.

In the low energy region of the lattice eigen-spectrum, the fundamental phonon branch is found with a band width which is fixed by the coupling of the atomic displacements. The superposition of two non-interacting phonon states yields an energy band at about twice the energy of the fundamental excitations. Provided that the lattice exhibits a significant nonlinearity, a second discrete branch in addition of the phonon branch is found to split from the two phonon band. By analogy with the theory of V. M. Agranovich, the states of the second discrete branch are named the biphonons. For the common case where the nonlinear contribution is not specially strong, the gap between the biphonon branch and the two phonon band is found to close at the center of the Brillouin zone while a pseudogap opens at the edge of the zone. It is proved that this pseudogap is a consistent property of the quantum lattice whose the nonlinear behavior is moderate. We enhance how the features of the pseudogap provide an accurate insight into the nature of the lattice nonlinearity.

When the biphonon gap opens over the whole lattice Brillouin zone, i.e., for a strong nonlinearity the biphonon states are found to have a finite correlation length on the condition

that the non-quadratic energy term varies as a power 4 of the atomic displacement. The biphonon is then a particle-like excitation. This result agrees with the findings of Ref. 2. Considering the cubic term in the non-quadratic energy, it is proved to involve a non-vanishing space correlation for the biphonon states. but the particle-like behavior of the biphonon is proved to remain the dominant part for a wide range of the nonlinear parameters. Similar features can also be proved for the triphonons and they are extended to the high energy multi-phonon states for which the extended contribution is shown to vanish. We propose to identify the Wannier transform of the multi-phonon bound states with a negligible extended part by the name of *quantum breathers*. This definition is consistent with the classical theory of the discrete breather modes<sup>12,13</sup> since the quantum breather wave function is spatially localized and no long range correlation occurs. When a biphonon gap closes at the center of the Brillouin zone, i.e., for a moderate nonlinearity the biphonon space correlation length diverges gradually when the wave vector decreases and thus the quantum breather does not hold.

The present paper is organized as follows. In Sec. II the model for the nonlinear discrete lattices is introduced and the computing method is detailed. Then it is tested for the linear lattices as well as for the  $\phi^4$  model<sup>2</sup>. In Sec. III our results are presented concerning the biphonon branch while in Sec. IV the space correlation of the phonon bound states are studied. Finally, these results are discussed in Sec. V.

## II. MODEL AND COMPUTING METHOD

A standard model for studying the nonlinear discrete lattices is formalized by the Klein-Gordon Hamiltonian:

$$H = \sum_i p_i^2/(2m) + V(x_i) - c \sum_{j=<i>} (x_i - x_j)^2. \quad (1)$$

At the node  $i$  of a translational invariant d-dimensional lattice, the atoms of mass  $m$  evolves in a local potential  $V$ , each of them being coupled to its nearest neighbors by an harmonic string which yields a force of magnitude  $c$  per unit length. The subscript  $j = < i >$  points at the first neighbors of the site  $i$ . For the small amplitude of the mass displacement around the mechanical equilibrium, the Taylor development of  $V$  gives  $V(x_i) = a_2x_i^2 + a_3x_i^3 + a_4x_i^4$ . The series is limited to the forth order but higher order terms can be taken into account

with no difficulty. The non-quadratic coupling terms are neglected in the present work.

Introducing the unitless operators  $P_i = p_i/\sqrt{m\hbar\Omega}$ ,  $X_i = x_i\sqrt{m\Omega/\hbar}$  where the frequency  $\Omega = \sqrt{2(a_2 - 2.c.d)/m}$  is for either a chain  $d = 1$  or a square lattice  $d = 2$  or else a cubic crystal  $d = 3$ , the Hamiltonian reads

$$H = \hbar\Omega \sum_i \frac{P_i^2}{2} + \frac{X_i^2}{2} + A_3 X_i^3 + A_4 X_i^4 + \frac{C}{2} X_i \cdot \sum_{j=\langle i \rangle} X_j \quad (2)$$

One finds the unitless coefficients:

$$A_3 = a_3 \sqrt{\frac{\hbar}{m^3 \Omega^5}}, \quad A_4 = a_4 \frac{\hbar}{m^2 \Omega^3} \quad \text{and} \quad C = \frac{4c}{m\Omega^2}. \quad (3)$$

For the harmonic lattice, i.e.,  $A_3 = 0$  and  $A_4 = 0$ , the Fourier transform of both the displacements and the momenta simplifies  $H$  into a sum of independent Hamiltonian  $h_q = \hbar\Omega(P_q^2/2 + \omega_q^2 u_q^2/2)$  where  $\omega_q = \sqrt{1 - 2C \sum_k \cos(q_k)}$  and where  $q_k$  is the unitless coordinate of the wave vector in the  $k^{\text{th}}$  direction of the lattice. The periodic boundary conditions fixe  $q_k = 2\pi l_k/L_k$  where  $L_k$  is the cells number in the  $k^{\text{th}}$  direction and  $l_k$  is an integer  $l_k \in [1, L_k]$ . Hence, using the standard harmonic oscillator theory, one finds the groundstate energy  $\frac{1}{2}\hbar\Omega \sum_q \sqrt{1 + 2C \sum_k \cos(q_k)}$  and the eigenvalues given by:

$$\Lambda_{\{n_q\}} = \hbar\Omega \sum_q \left(n_q + \frac{1}{2}\right) \sqrt{1 + 2C \sum_k \cos(q_k)} \quad (4)$$

where the  $n_q$ 's are the quanta number that take integer values from 0 to the infinity and that fix the energy contribution of the mode  $q$ . The eigenvalue  $\Lambda_{\{n_q\}}$  is wholly determined by the set of the  $S$  integers  $\{n_q\}$ .

For the nonlinear case, the aforementioned procedure is no longer simple because the non-quadratic terms, i.e.,  $(A_3 u_i^3 + A_4 u_i^4)$  yield a non-trivial coupling between the  $h_q$  operators. Thus we proceed differently as mentioned in the introductory section of the paper. The starting point is the eigenvalue problem for a single oscillator  $h_i = \hbar\Omega(P_i^2/2 + u_i^2/2 + A_3 u_i^3 + A_4 u_i^4)$ . The introduction of the Bose-Einstein operators  $a_i^+ = \sqrt{2}(P_i + u_i)$  and  $a_i = \sqrt{2}(u_i - P_i)$  transforms  $h_i$  into

$$h_i = \hbar\Omega \left[ a_i^+ a_i + \frac{1}{2} + \frac{A_3}{\sqrt{8}} (a_i^{+3} + a_i^3 + 3a_i^+ a_i^2 + 3a_i^{+2} a_i + 3a_i^+ + 3a_i) + \frac{A_4}{4} (a_i^{+4} + a_i^4 + 4a_i^{+3} a_i + 4a_i^+ a_i^3 + 6(a_i^{+2} a_i^2 + a_i^{+2} + a_i^2 + 2a_i^+ a_i) + 3) \right]. \quad (5)$$

Expanding the operator  $h_i$  on the Einstein states, i.e.,  $|n, i \rangle = \frac{1}{\sqrt{n!}} a_i^{+n} |\emptyset_i \rangle$  for all  $n \in \{0 \dots N-1\}$  gives a matrix  $\mathcal{M}$  of rank  $N$ . Upon each line of  $\mathcal{M}$ , one finds the nonzero coefficients:

$$\begin{aligned}
\mathcal{M}_{n,n} &= \frac{3}{2}A_4n^2 + n(3A_4 + 1) + \frac{3}{4}A_4 + \frac{1}{2} \\
\mathcal{M}_{n,n+4} &= \frac{1}{4}A_4\sqrt{(n+4)(n+3)(n+2)(n+1)} \\
\mathcal{M}_{n,n+3} &= \frac{1}{\sqrt{8}}A_3\sqrt{(n+3)(n+2)(n+1)} \\
\mathcal{M}_{n,n+1} &= \frac{3}{\sqrt{8}}A_3\sqrt{(n+1)^3} \\
\mathcal{M}_{n,n+2} &= \frac{1}{4}A_4(4n+6)\sqrt{(n+2)(n+1)}.
\end{aligned} \tag{6}$$

When the cutoff  $N$  tends to infinity the Einstein states form a base for the space of the onsite states and the Schrödinger problem for the Hamiltonian  $h_i$  is equivalent to the diagonalization of  $\mathcal{M}$ . In Fig. 1(a), the diagonalization of  $\mathcal{M}$  is compared with the semi-classical quantization<sup>14</sup> for the case of a *He* atom embedded into the double-well potential  $V = 16E_d/b^4x^2(x-b)^2$  where  $E_d$  is the top of the energy barrier and  $b$  is the distance between the two minima. The very good agreement proves the efficiency of the diagonalization method even for a non-monotonous onsite potential. The corresponding parameters in Eq. (5) are  $A_3 = -0.09496$ ,  $A_4 = 0.00451$  and  $\hbar\Omega = 0.02886eV$ .

As shown in Fig. 1(b), the eigenvalues of  $h_i$  can be computed with a great accuracy provided the cutoff  $N$  is large enough. Indeed, each eigenvalue is proved to converge to a limit value when  $N$  increases. In what follows, for each calculation,  $N$  is fixed in order that increasing again the cutoff does not yield any modification of the first eigenvalues to machine precision. In that sense, the calculation is exact for the low energy states. Arranging the  $h_i$  eigenstates by increasing order of their eigenvalues, the  $\alpha^{\text{th}}$  eigenstate is denoted  $\phi_{\alpha,i}$  and its eigenvalue is  $\gamma(\alpha)$ . The degeneracy of a given eigenvalue might involve different indices for the same eigenvalue. In Fig. 2, for different sets of the non-quadratic coefficients, i.e.,  $A_3$  and  $A_4$  the bracket of the displacement operator  $\langle \phi_{\alpha_i} | X_i | \phi_{0_i} \rangle$  is plotted versus the rank  $\alpha$  of the eigenstate  $\phi_{\alpha_i}$ . For the purpose of a further discussion Sec. IV, it is noteworthy that the absolute value of this bracket is maximum at the first eigenstate  $\alpha = 1$  and it shrinks to

zero very fast by increasing  $\alpha$ . In addition, for the low energy level  $\alpha$  and for all values of  $A_4$  and  $A_3$ , the quantity  $\langle \phi_{\alpha_i} | X_i | \phi_{0_i} \rangle$  is found to have no zero when  $\alpha$  is a odd number whereas for the even  $\alpha$ 's it only vanishes at  $A_3 = 0$  for all  $A_4$ .

We now treat the case of the interacting atoms. By denoting  $i$  the  $S$  sites of the lattice ( $S = \prod_{k=1}^d L_k$ ), the onsite state products  $\prod_i \phi_{\alpha_i}$  form a complete orthogonal base for the states of the network.

In order to reduce the computer memory requirement, one takes advantage of the translation invariancy by introducing the Bloch wave formulation for the state products with at least a nonzero  $\alpha_i$ , i.e.  $\prod_i \phi_{\alpha_i \neq 0, i} \prod_i \phi_{0, i}$ . Among those states some equivalent classes can be constructed in which each state results of a lattice translation applied to an other state of the same class. Retaining only one element for each translation class, the representing state of the class is identified by the series of its  $\alpha_i$ 's, that is denoted  $[\prod_b^n \alpha_p]$  where the lattice vector  $p$  points at the sites where  $\alpha_p \neq 0$  and  $n$  is the number of those sites that bear the local excitations.

For each equivalent class, a Bloch wave can be written as follows:

$$B_{[\prod_b^n \alpha_b]}(q) = \frac{1}{\sqrt{A_{[\prod_b^n \alpha_b]}}} \sum_j e^{-iq \cdot j} \prod_b \phi_{\alpha_b, b-j} \cdot \prod_{l \neq b} \phi_{0, l-j} \quad (7)$$

where  $A_{[\prod_b^n \alpha_b]}$  insures the normalization. Some attention must be payed to the possible translation symmetry of the state products that may be higher than the lattice symmetry. Indeed, for a given state there may be a lattice vector  $t$  that verifies  $\prod_b \phi_{\alpha_b, b} \cdot \prod_{l \neq b} \phi_{0, l} = \prod_b \phi_{\alpha_b, b-t} \cdot \prod_{l \neq b} \phi_{0, l-t}$  with coordinates  $t_k$  such as  $t_k < L_k$ . It implies that  $A_{[\prod_b^n \alpha_b]} = S \cdot \prod_{k=1}^d (L_k/t_k - fc(L_k/t_k))$  where  $fc(L_k/t_k)$  is the fractional portion of the ratio  $L_k/t_k$ . Then the Bloch wave can only takes the wave momentum  $q$  such as  $q_k = 2\pi p_k/L_k = 2\pi p'_k/t_k$  where  $p_k$  and  $p'_k$  are some integers. To avoid such complication, one could choose to work with a lattice where each  $L_k$  is a prime number.

The set of states  $\{\prod_i \phi_{0, i}, B_{[\prod_b^n \alpha_b]}(q)\}_{q, n < N_{oe}}$  including the uniform state  $\prod_i \phi_{0, i}$ , form a truncated basis where the number  $N_{oe}$  fixes the upper number of the onsite excited states that are considered into the Bloch waves  $B_{[\alpha_b]_n}$ . When the coupling  $C$  is negligible, these states are the eigenstates of the Hamiltonian  $H = H_0$ . For a moderate amplitude of  $C$ , they should be some good approximates of the  $H$  eigenstates. As seen before for the single site problem, the truncation of the base with a high enough energy cutoff may be expected not to affect the calculation of the low energy eigenstates. That assumption is verified for the

harmonic lattice by comparing our calculations with the exact formula Eq. (4) (see Fig. 3 and below in the text for further details). As the study is focussed on the low energy excitations of the large size systems, the uniform states  $\psi_\alpha = \prod_i \phi_{\alpha,i}$  with  $\alpha > 0$  are not considered into the calculation since the difference  $\langle \psi_\alpha | H | \psi_\alpha \rangle - \langle \psi_0 | H | \psi_0 \rangle$  increases linearly with  $S$  (provided the groundstate of  $h_i$  is not degenerate).

Since the Bloch waves with different  $q$  are not hybridized by the lattice Hamiltonian  $H$ , the Schrödinger equation can be solved severally for each value of  $q$ . Expanding the Hamiltonian  $H$  onto the onsite state product Bloch waves is done analytically and gives a matrix  $\mathcal{B}(q)$  the coefficients of which are written as follows

$$\langle B_{[\prod_b^n \alpha_b]}(q) | H | B_{[\prod_b^m \beta_b]}(q) \rangle = \frac{1}{\sqrt{A_{[\prod_b^n \alpha_b]} A_{[\prod_b^m \beta_b]}}} [\prod_i \delta_{\alpha_i, \beta_i} \sum_i \gamma(\alpha_i) - \frac{C}{2} \sum_{l,j} \exp(-iq \cdot j) \cdot \sum_{k=\langle l \rangle} sc(\alpha_l, \beta_{l+j}) \cdot sc(\alpha_{l+k}, \beta_{l+k+j}) \prod_{i \neq l, l+k} \delta_{\alpha_i, \beta_{i+j}}] \quad (8)$$

where the bracket  $\langle \phi_{\alpha_i} | X_i | \phi_{\beta_i} \rangle$  is denoted  $sc(\alpha_i, \beta_i)$  and is given by

$$sc(\alpha_i, \beta_i) = \frac{1}{\sqrt{2}} \sum_{l=0}^N \langle \phi_{\alpha,i} | l, i \rangle (\sqrt{l+1} \langle l+1, i | \phi_{\beta,i} \rangle + \sqrt{l} \langle l-1, i | \phi_{\beta,i} \rangle). \quad (9)$$

The eigenvalues of  $\mathcal{B}(q)$  are computed numerically with an exact Householder method<sup>15</sup>. For convenience, we fix the arbitrary rule such as the onsite state products verify  $\sum_i \alpha_i \leq N_{oe}$  for each state product waves. Hence the only value of  $N_{oe}$  fixes the precision of the calculation which is compared with the analytical expression of the eigenvalues Eq. (4) for a purely quadratic Hamiltonian. For a 1D chain, that comparison is done in Fig. 3 where are reported the computing results for the different  $N_{oe}$  values, e.g. ,  $N_{oe} = 2$ ,  $N_{oe} = 3$  and  $N_{oe} = 4$ . The precision increases with  $N_{oe}$  but the computing time increases too, so for the large size system the numerical calculations were performed with  $N_{oe} \leq 5$  for the one-dimensional chains whereas for two dimensions  $N_{oe} \leq 3$ . For the 2D case the accuracy is worse than for 1D. It is remarked that for achieving a fixed precision, the required  $N_{oe}$  increases with both the coupling  $C$  and the size  $S$  due to the non-conservative quanta terms  $a_i^+ a_j^+$  or  $a_i a_j$  that come from the realistic coupling.

In Fig. 4, for a small length chain  $S = 4$ , our calculation is compared to the one performed in Ref. 2 with a very good agreement for the low energy states. The results of Ref. 2 have

been reproduced by hand with a precision of at least 5%. Writing our parameters as some functions of the model parameters of Ref. 2 gives:  $\sqrt{2(w + \eta)} \rightarrow \Omega$  and  $-\eta \rightarrow C.\Omega^2$ ,  $v \rightarrow A_4.\Omega^3$  and  $A_3 = 0$ . In Ref. 2, the Schrödinger equation was solved by a diagonalization of the matrix issued from expanding the Hamiltonian  $H$  over the state products of the onsite Einstein base  $\Pi_i|n, i \rangle$ . Although the Bloch waves formulation which is introduced in the present section permits to take advantage of the translational symmetry of the lattice and subsequently to divide the rank of the eigenvalue problem by a factor  $S$ , i.e., the size of the lattice. So the large systems can be treated with typical size around  $S = 30$  atoms for the 1D chains and  $S = 13 \times 13$  atoms for the 2D lattices. These performances could be improved again by computing the diagonalization of the matrix  $\mathcal{B}(q)$  with a non-exact numerical procedure which have not been done in the present work.

### III. GAP AND PSEUDOGAP IN THE OPTICAL PHONON SPECTRUM

For different values of the nonlinear coefficients  $A_3$  and  $A_4$ , we first investigate the vibration energy spectrum of a 1D chain. The 2D lattice spectrum is treated at the end of the present section.

When the non-quadratic part of the lattice energy is negligible the eigen-spectrum of the Hamiltonian is composed of the fundamental optical branch of the phonon states and the branches due to the linear superpositions of these phonons. The latest branches are staked together into distinct bundles, each of them filling in a compact range of energy. In Fig. 5 and following ones, each eigenvalue of the finite size network Hamiltonian  $H$  is represented by a single circle symbol. The individual eigenenergy participate to the different branches of the energy spectrum. The phonon branch is marked with the tag  $\{1\}$  while the branches that are due to the linear superposition of two phonon states are pointed out by the tag  $\{11\}$ . For the convenience of the discussion, the states that belong to the bundle  $\{11\}$  are named the free phonons. For a macroscopic system, the bundle  $\{11\}$  covers a dense range of energy and forms a continuous band. The width of an optical phonon branch being physically of a few percent of the elementary excitation energy, the unitless coupling  $C$  is fixed to  $C = 0.05$  in the model Eq. (2) which gives for the width  $\Delta_1$  of the phonon branch  $\Delta_1 \approx 10\%$  of the phonon energy.

When the nonlinearity is significant, the parameters  $A_3$  and  $A_4$  are no longer negligible

in Eq. (2). Then, as shown in the left-hand inserts of the figures 5 (a) and 6 (a), the phonon branch shows no qualitative change in comparison with the fundamental optical branch of a quadratic lattice. Although an isolated spectral branch is found in addition to the phonon branch and its combination tones (see Figs. 5(a) and 6(a) and the magnifications in their right-hand inserts). In Fig. ??, varying artificially the coupling  $C$  to the trivial case  $C = 0$  demonstrates that the additional branch coincides with the energy of the onsite state product  $B_{[\alpha]_1}$  with a single onsite excitation  $\alpha = 2$ . In Fig. 5 and the next ones, the additional branch is marked with the single tag  $\{2\}$ . By analogy with the biphonon theory, that branch is identified as the energies of the biphonon states. Similar results are found for the branch of the triphonon states pointed by the tag  $\{3\}$  in Fig. ?. The reason for these isolated branches is that the onsite Hamiltonian  $h_i$  eigenvalues  $\gamma_{\alpha>1}$  do not match the linear fit given by  $(\gamma_1 - \gamma_0)n + \gamma_0$ . The differences  $\gamma_{\alpha>1} - [(\gamma_1 - \gamma_0)n + \gamma_0]$  are the result of the nonlinearity of the onsite potential  $V$  in Eq. (2). These differences involve some gaps in the  $C = 0$  spectrum which is composed of the energies of the waves  $B_{[\Pi_b^n \alpha_b]}$ . A moderate inter-site coupling induces an hybridization between the states  $B_{[\Pi_b^n \alpha_b]}$  but the largest gaps of the  $C = 0$  spectrum remain (Fig. ??).

The raising of the degeneracy of the states  $B_{[11]}$  (the number of degenerated states with the same energy  $2\gamma(1) + (S - 2)\gamma(0)$  is  $S(S - 1)/2$ ) yields a bundle of branch which energy corresponds to the linear superposition of two single phonon states, the free pair of phonons. In the figure Fig. ??, other bundles are pointed out by the tags  $\{21\}$  and  $\{111\}$  for a higher energy range. These branches coincide with the energy of the states  $B_{[21]}$  and  $B_{[111]}$  at zero coupling. For a macroscopic lattice, the bundles  $\{21\}$  and  $\{111\}$  contribute to the dense energy spectrum as well as  $\{11\}$ . They can be viewed as the results of the unbound associations of either a biphonon state with a phonon state or the three phonon states, respectively.

In Figs. 5(a) and 6(a), for different parameters, the eigen-spectra show a gap between the biphonon and the two phonon band. By measuring the energy of the biphonon with reference to the free phonons for the same wave vector  $q$ , a binding energy of the biphonon is defined. A positive binding energy occurs when the onsite potential  $V$  hardens Fig. 5(a) whereas a softening yields a negative binding energy Fig. 6(a). The biphonon energy gap is equal to the minimum of the absolute value of the biphonon binding energy with respect to the wave vector  $q$ . The biphonon gap reveals the strength of the nonlinearity in the sense

that when the biphonon gap overpasses the width of the phonon branch (as it is the case in Figs. 5(a) and 6(a)) it clearly indicates a significant contribution of the non-quadratic terms in the energy. While in Figs. 5(a) and 6(a) the biphonon gap opens over the whole Brillouin zone of the lattice it is found that when the nonlinearity is not very strong the binding energy of the biphonon states vanishes at the center of the Brillouin zone (Figs. 5(b) and 6(b)). Although at the edge of the zone the binding energy is comparable to the width of the phonon branch  $\Delta_1$  (inserts in Figs. 5(b) and 6(b)). Consequently, a pseudogap is yielded when the non-quadratic energy has same magnitude than the inter-site coupling. In this regime, the biphonon excitations exist only at the edge of the Brillouin zone while they are dissociated into a pair of free phonons at center of the zone. With similar results, other calculations have been performed for different parameters. They revealed that the biphonon pseudogap is a generic feature of the lattices where the onsite nonlinearity contribution is of the order of the inter-site coupling and it opens consistently at the edge of the Brillouin zone, even though the coupling sign is changed. There is a wave vector threshold  $q_t$  below which the biphonon gap becomes negligible for  $q < q_t$ . The binding energy of the biphonon decrease gradually with  $q$  and the biphonon dissociates into a free phonon state when  $q < q_t$  (Figs. 5(b) and 6(b)). For a weak nonlinearity, the binding energy of the biphonon is negligible for all  $q$  wave vectors but strictly speaking the pseudogap opens as soon as the nonlinear coefficients are non-zero with a width which characterizes the nonlinear energy contribution.

In Fig. ??, the low energy eigenvalues of  $H$  are plotted versus the coupling amplitude  $C$ . The triphonon branch is pointed out by the tag {3} and it is found to merge with the free phonon bands for a certain threshold of  $C$  (Figs. ??(a) and ??(b)). The threshold depends on both coefficients  $A_3$  and  $A_4$  and it is different for each phonon bound state because of the anharmonicity of  $h_i$  eigenvalues which yields different surrounding gaps for the triphonon and the biphonon branches. For every distribution of gaps for the biphonon and the triphonon, there is a single set of the nonlinear parameters  $A_3$  and  $A_4$  that correspond unequivocally. So in principle, if a spectroscopic analysis reveals the biphonon and the triphonon resonances, it is sufficient for inverting our numerical treatment and so determining the correspondent nonlinear parameters.

In Fig. 7, the diagonalization of a two-dimensional lattice Hamiltonian is performed for  $A_3 = 0$  and for different values of the parameter  $A_4$ . The coupling amplitude is such as the

phonon band width  $\Delta_1$  is a few percent of the elementary excitation branch so by estimating that  $\Delta_1 \approx 2.d.|C|$  the value of the unitless coupling is fixed around  $C = 0.025$ . The group symmetry of the square lattice is used for speeding up the calculations. A two-dimensional lattice with size  $S = 13 \times 13$  is studied. In the biphonon energy range, a gap opens over the whole Brillouin zone when  $A_4$  is large enough (top of Fig. 7) whereas the gap is closed at the center of the Brillouin zone when  $A_4 = 0.025$  (bottom of Fig. 7). In the latter case, a pseudogap is found to open around  $q = \pi[11]$  and the width of the pseudogap has same order of magnitude than the phonon band width. These both quantities can be compared in the right hand side inserts in Fig. 7 that show the profile of the energy spectrum along the direction  $[11]$  of the reciprocal lattice. By reason of the likeness between the two-dimensional lattice and the one-dimensional results, a pseudogap is expected for all lattice dimensions when both the inter-site coupling and the onsite nonlinearity have a comparable magnitude. The order of magnitude for the pseudogap is the same in Fig. 5 and Fig. 7.

#### IV. CORRELATION PROPERTIES OF THE MULTI-PHONON STATES

In the present part, the study is focussed on the space correlation of the displacement operators for the Hamiltonian eigenstates  $\Phi$  in the one-dimensional lattices. The space correlation function is defined as follows:

$$f(\Phi, n) = \sum_l \langle \Phi | X_l X_{l+n} | \Phi \rangle - \langle \Phi | X_l | \Phi \rangle \langle \Phi | X_{l+n} | \Phi \rangle \quad (10)$$

where  $n$  is the unitless distance ( $n > 0$ ). For a quadratic Hamiltonian,  $A_4 = 0$  and  $A_3 = 0$  it is easily verified that  $f(\Phi, n) = \sum_q \cos(q n)$  for a state  $\Phi$  which is composed of the linear superposition of the single phonon states whose the wave momenta are given by the series of the  $q$ 's. The correlation function for the eigenstates of a quadratic Hamiltonian reveals a space modulation with a constant amplitude. At  $q = 0$ , the function  $f(\Phi, n)$  is a non-zero constant for all values of  $n$ .

Before describing our results, it is convenient to compute analytically the function  $f(\Phi, n)$  for the onsite excitation product Bloch waves Eq. 7 with only one onsite excitation of order  $\alpha$ . In a 1D chain with a prime number of site these states writes:

$$B_{[\alpha]}(q) = \frac{1}{\sqrt{S}} \sum_j e^{-iq \cdot j} \phi_{\alpha, j} \cdot \prod_{l \neq 0} \phi_{0, l+j}. \quad (11)$$

At the uncoupled limit of the network ( $C = 0$ ), the onsite excitation Bloch waves are found to correspond to the  $H$  eigenstates (see Fig. ?? and text in Sec. III). Then the space correlation function is given by:

$$f(B_{[\alpha]}(q), n) = 2sc(\alpha, 0)^2 \cos(q n) - \frac{(sc(\alpha, \alpha) - sc(0, 0))^2}{S} \quad (12)$$

for all  $n > 0$  and where  $sc(\alpha, \beta) = \langle \phi_{\alpha_i} | X_i | \phi_{\beta_i} \rangle$  as in Eq. 9. The constant term in the right hand side of Eq. 12 vanishes when the size of the chain  $S$  increases. In the numerical computations that are presented below for the finite size lattices, the contribution of the constant in Eq. 12 is removed in order to approach the behavior of the infinite size lattices. Another point which is noteworthy in Eq. 12 is that, in general, the displacement operators are correlated for a given state  $B_{[\alpha]}$ . Indeed the bracket  $sc(\alpha, 0)$  that is plotted in Fig. 2 (for different nonlinear parameters) is usually not zero and the function  $f(B_{[\alpha]}(q), n)$  exhibits a space modulation of amplitude  $cor_\alpha = 2sc(\alpha, 0)^2$ . Strictly speaking the bracket  $sc(\alpha, 0)$  is zero only for the even values of  $\alpha$  on condition that  $A_3 = 0$ . The coefficients  $cor_\alpha$  are given in table Tab. I for the values of the coefficients  $A_4$  and  $A_3$  that have been used in the previous calculations presented in Figs. 5 and 6.

The function  $f(\Phi, n)$  is plotted in Figs. 8-11 for the model parameters corresponding to the spectrum calculations in Figs. 5-6 and for some eigenstates of  $H$  that are either the phonon, the biphonon or the triphonon states. For each state, the function  $f(\Phi, n)$  is computed for several wave vectors of the lattice Brillouin zone. The comparison of our calculations at  $C > 0$  with the formula in Eq. 12 demonstrates that the long range behavior of the space correlation function for the phonon states ( $\alpha = 1$ ) as well as for the multi-phonon bound state of order  $\alpha$  ( $1 < \alpha < 4$ ) is fixed by the value of  $cor_\alpha$ . This property is proved to hold provided that the spectral branch of the  $\alpha$ -phonon bound state is separated from the rest of the energy spectrum by some gaps. In Figs. 8(a)-11(a), the correlation function of the single phonon states shows a modulation which extends over the whole lattice as it is the case for the pure quadratic lattice. For the large values of the distance, i.e.,  $n > 2$  the variations of  $f(\Phi, n)$  are similar to the ones given by the formula of Eq. 12. Indeed the amplitude of the modulations is roughly given by the coefficient  $cor_\alpha$  for  $\alpha = 1$  (see Tab. I). The correlated character of the phonon states is thus related to the feature of the onsite excitation Bloch wave  $B_{[1]}$  and more precisely to the fact that the onsite displacement

operator generates an overlap between the first eigenstate of the onsite Hamiltonian  $h_i$  and the onsite groundstate  $\phi_{0,i}$ . The reason for such an agreement between the properties of the phonon states and  $B_{[1]}$  is simply the weak inter-site coupling of the optical lattices. Consequently it is also true for the pure quadratic lattice as it can be checked by comparing the exact formula  $f(\Phi, n) = \cos(q n)$  for the single phonon state of wave momentum  $q$  in a quadratic chain with the equation Eq.12, noting that  $sc(1, 0) = 1/\sqrt{2}$ .

In truth, provided the biphonon gap opens over the whole Brillouin zone there is no conceptual difference between the biphonon states and the phonon states since they all come from the raising of the translational degeneracy of the onsite Hamiltonian  $h_i$  eigenstates  $|\phi_{\alpha_i}\rangle$ . As a consequence, when the hybridization with the free phonon pairs is weak, i.e., a biphonon gap opens, one may expect that the correlation properties of the biphonon states follow the same behavior than the phonon states ones in the sense that the long range modulations of  $f(\phi, n)$  have same magnitude than the coefficient  $cor_2$ . It can be observed in Figs. 8(b) and 9 (b) that it does indeed, whereas in Figs. 10(b) and 11 (b) it does not because the biphonon gap closes for the small wave vectors  $q$ . In Fig. 8(b), the space correlation function vanishes for the large values of the distance  $n$  for all the wave vectors as  $cor_2$  equals zero (see Tab.I). In Fig. 9 (b), the amplitude of the long range modulations is around  $10^{-2}$  which is the order of magnitude of  $cor_2$  for the corresponding nonlinear parameters in Tab.I. The agreement between the order of magnitude of the coefficient  $cor_\alpha$  and the long range modulations of the space correlation function of the multi-phonon bound state can be checked again for the triphonon state in Figs. 8(c) and 9(c). Actually, the coefficient  $cor_\alpha$  is a good indicant of the long range space correlations of the displacement operators for the  $\alpha$ -phonon bound states on the condition that their hybridization with the free phonon is negligible. In other words, when  $cor_\alpha = 0$  the multi-phonon bound states of order  $\alpha$  exhibit a finite length scale provided the  $\alpha^{th}$  discrete branch of the energy spectrum is isolated in the energy spectrum.

As indicated in Fig. 2 and Tab. I the factors  $sc(\alpha, 0)$  and subsequently  $cor_\alpha = 2sc(\alpha, 0)^2$  decrease very fast with the order of the onsite excitation  $\alpha$ . By extension of our results about the space correlations of the  $\alpha$ -phonon bound states with  $\alpha < 4$  to the high energy multi-phonon bound states, it is expected that the latest have a finite correlation length provided their energy branch remains separated from the linear combination band of the lower energy states, i.e., from the free phonons as well as from the combinations of the lower

order multi-phonon bound states as for the band {21} in Fig. ???. For the specific case of a quartic onsite potential, i.e.,  $A_3 = 0$  and  $A_4 > 0$  the even values of  $\alpha$  verify  $cor_\alpha = 0$  so the corresponding  $\alpha$ -phonon bound states, whatever are their energies are also expected to show a finite correlation length when the gap of the  $\alpha^{th}$  branch opens.

The multi-phonon bound states that have a finite correlation length exhibit a singular feature which is worth to characterize more precisely. Noting  $|\Phi_\alpha(q)\rangle$  the  $\alpha$ -phonon states of the discrete spectral branch  $\alpha$  ( $1 \leq \alpha$ ) with a wave momentum  $q$ , the wave function of the associated Wannier transform writes

$$|Wt_\alpha(i)\rangle = \frac{1}{\sqrt{S}} \sum_q e^{-jq \cdot i} |\Phi_\alpha(q)\rangle \quad (13)$$

where the subscript  $i$  indicates the lattice site where is centered the wave function of the Wannier transform. One points out that  $|Wt_\alpha(i)\rangle$  is quasi-periodic in time since it is constructed with the linear superposition of the eigenstates  $|\Phi_\alpha(q)\rangle$  that are time periodic solutions of the Shrödinger equation. When the dispersion of the branch  $\alpha$  shrinks to zero, i.e., the alpha-phonon bound states are tunneling-less and the energy of the  $|\Phi_\alpha(q)\rangle$  is a constant which is independent of  $q$ , so the corresponding Wannier transform becomes a time-periodic modes. As we found that the space correlation properties of  $|\Phi_\alpha(q)\rangle$  are rather well approached by the ones of the single excitation Bloch waves  $B_{[\alpha]}(q)$ , the later is introduced in Eq. 13 which gives simply the state product  $\phi_{\alpha,i} \prod_{l \neq i} \phi_{0,l}$ . Then the space localization of the related Wannier state appears clearly since only one site bears the excitation  $\alpha$ . This remark holds for all the discrete branch of the energy spectrum even for the fundamental phonon branch. In addition, considering the Wannier transform for a given branch  $\alpha$  and for two distinct sites  $m$  and  $n$  ( $|n - m| \gg 1$ ) of the lattice, the product  $X_n X_m$  of the displacement operators that correspond to these sites yields an overlap between the two Wannier transforms so that:

$$\langle Wt_\alpha(n) | X_n X_m | Wt_\alpha(m) \rangle \approx cor_\alpha / 2 \quad (14)$$

where the symbol ( $\approx$ ) is replaced by ( $=$ ) when the Wannier transform is performed onto the single excitation Bloch waves  $B_{[\alpha]}(q)$  instead of the  $\alpha$ -phonon bound states. Therefore when  $cor_\alpha \neq 0$  a long range space correlation occurs between the two Wannier states localized at different sites whereas when  $cor_\alpha = 0$  no long range correlation is yielded.

The Wannier transforms of the multi-phonon bound states that have a finite correlation length for all  $q$  are thus characterized by three properties: first, they are spatially localized; Second, they are time quasi-periodic and third, they show no long range correlation. Here we propose to identify the states issued from the Wannier transform of the multi-phonon bound states that have a finite correlation length (for all  $q$ ) as the quantum breather modes<sup>2</sup> of the lattices. The classical counterparts of the quantum breathers would be the breather solutions for the classical nonlinear discrete lattice, first enhanced by A. J. Sievers and S. Takeno<sup>12</sup>. These classical breather solutions have two important features that are first their spacial localization and second their time periodicity with a frequency that is out of both the linear classical phonon branch and its resultant harmonic bands (for an exact proof see Ref. 13). Because of their spacial localization and their time quasi-periodicity the Wannier transforms of the particle-like multi-phonon states are identified as the quantum breathers of the Klein-Gordon model. The absence of long range correlation appears as an additional property of the quantum breather with respect to the classical theory of breathers because the space correlation of the quantum states has no equivalent in classical mechanics. As a summary and according to the definition that we propose, one can retains that a quantum breather is constructed from the Wannier transform of the multi-phonon bound states of the discrete  $\alpha^{th}$  branch that have a finite space correlation length which is equivalent to the condition that this branch is isolated in the energy spectrum and that  $cor_\alpha = 0$ .

The study is now concentrated on the breathing behavior of the biphonon states. In Fig. 8(b), the biphonon states have a finite length scale because the cubic contribution in the non-quadratic energy is negligible and the biphonon gap opens. A quantum breather can thus be constructed from the biphonon branch with a quasi-periodic time evolution. For a non-zero cubic term in the onsite potential as it is the case in Fig. 9, the table Tab.I gives a non-zero factor  $cor_2$  and consequently the correlation function do no longer vanish above a certain distance. Nevertheless the amplitude of the long range modulations keeps much weaker for the biphonon than for the phonon states ,i.e., less than 3%. Consequently the biphonon states can be though to have a weak spatially correlated contribution whereas their main part comes from a non-correlated state. For a reasonable nonlinear contribution in  $H$ , i.e., a biphonon gap which does not overpass 20% percent of the elementary excitation energy, it has been checked that the coefficient  $cor_2$  remains inferior to few percent of  $cor_1$ .

So the previous interpretation of the results in Fig. 9 can be considered as relevant for a wide class of nonlinear lattices where a biphonon gap opens with  $A_3 \neq 0$ . The Wannier transform associated with the biphonon states have a weak space correlated contribution which becomes insignificant for the small values of  $A_3$ . When  $A_3 \neq 0$  and the branch of the  $\alpha$ -phonon bound states is isolated into the energy spectrum, these states show the same property as the biphonon that is a dominant non-correlated contribution is superposed to a weak correlated part. For the reasonable values of  $A_3$  this correlated part becomes negligible for  $\alpha > 3$  as indicates the corresponding value of  $cor_\alpha$  which is much less than 1% of  $cor_1$  (Tab.I). Thus even for  $A_3 \neq 0$  it is possible to construct some quantum breathers from the high energy discrete branch that may fall into some energy gap.

For a closing biphonon gap, a pseudogap was found to persist at the edge of the lattice Brillouin zone Sec. III. It is shown in Fig.10(b) that the biphonon state have a finite length scale only for the range of the wave vectors where the pseudogap is opened. Then because of the hybridization with the two phonon states the biphonon states at  $q \approx 0$  have a non-vanishing space correlation function. The correlation length of the biphonon at small  $q$  diverges and overpasses the finite lattice size. So the Wannier transform of the biphonon states shows a long range correlation. As a consequence, the quantum breather does not persist in the pseudogap regime which is consistent with the classical theory of breathers whose the orbital frequencies must fall out of the linear classical phonon branch and its resultant harmonic bands. The same is found in Figs.11(b) for a non zero cubic term which makes the onsite potential soften.

Analyzing the curvature of the biphonon branch for different lattices with distinct biphonon gaps shows that the larger is the biphonon gap the weaker is the curvature of the branch. It reveals that the tunneling of a multi-phonon bound states depends on its ability to dissociate into a free phonon states. So when the multi-phonon gap is large into the spectrum the quantum tunneling is weak and the branch is dispersive-less. The time quasi-periodicity of the corresponding quantum breather becomes a strict periodicity because the eigenvalues of the multi-phonon states do not depends on the wave momentum. In the high energy region of the spectrum, it is thus expected to find some time periodic quantum breather modes.

## V. PERSPECTIVES

In the present paper, the pairing of the phonon states in the nonlinear optical lattices has been considered with numerics. In the energy spectrum, a pseudogap is proved to open as soon as the nonlinearity is significant, i.e., comparable to the width of the fundamental optical phonon branch because of the pairing of the phonon states. The pseudogap opens systematically at the edge of the lattice Brillouin zone. Furthermore, when the magnitude of the nonlinearity overpasses the width of the phonon branch, the phonon bound pairs have an energy branch that is separated from the rest of the spectrum by some gaps that open over all the Brillouin zone. Then from the biphonon states, a quantum breather excitation is yielded though the nonlinear energy contribution reduces to a quartic term. For a general form of the nonlinearity, these results have been extended to the high energy multi-phonon bound states that are expected to give some quantum breathers provided their branch are isolated into the energy spectrum.

The non-quadratic coupling terms such as  $(X_i X_j^2)$  or else  $(X_i^2 X_j^2)$  have been neglected in the present work Eq.2. They are actually found not to modify qualitatively our results and their outcome is equivalent to the rescaling of the quadratic coupling amplitude  $C$ , provided their coefficients in Eq. 2 do not overpass 20% of  $C$ .

To conclude, the experimental evidence for the biphonon pseudogap may be expected. For instance, the Raman analysis of the high pressure molecular  $H_2$  shows a pressure-induced bound-unbound transition of the bivibron<sup>16</sup> around 25 GPa. Right at this transition, the inelastic scattering of neutron might confirm the presence of a pseudogap in the energy spectrum. More generally, as the spectral features of the phonon bound states were found to be unambiguously related to the nonlinear terms of the energy development with respect to the atomic displacements, measuring the biphonon and the triphonon spectral branch should allow to go beyond the well-known phonon analysis and to quantify the nonlinear part of the atomic interactions for some fixed temperature and external pressure instead of limiting the energy development to the quadratic terms. In a same manner, the empirical potentials that are used for describing the atomic interactions are adapted for fitting the phonon frequencies and thus the weak amplitude of the atomic displacements. Modifying such potentials in order to be valid for the biphonon frequen-

cies would extend the validity of the empirical potentials to the large atomic displacements<sup>17</sup>.

I gratefully acknowledge the financial supports from both the Trinity College (University of Cambridge, UK) and the Mathematics Institute ( University of Warwick UK). The numerics was performed partly on the computers of the Department of Applied Mathematics and Theoretical Physics (University of Cambridge) and partly on the computers of the Service de Recherches de Métallurgie Physique (CEA/DEN/DMN, France). Many thanks are addressed to Robert S. MacKay and Serge Aubry for the enlightening discussions we had about the breather theory.

- 
- <sup>1</sup> V.M. Agranovich, *Spectroscopy and excitation dynamics of condensed molecular systems*, chp. 3, North-Holland publishing company (1983), pp. 83-138.
  - <sup>2</sup> W.Z. Wang, J.T. Gammel, A.R. Bishop and M.I. Salkola, *Phys. Rev. Lett.* **76**, 3598 (1996).
  - <sup>3</sup> V.M. Agranovich, *Soviet Physics - Solid State* **12**, 430 (1970).
  - <sup>4</sup> V.M. Agranovich and I. I. Lalov, *Soviet Physics - Solid State* **18**, 1148 (1976).
  - <sup>5</sup> V.M. Agranovich, *Spectroscopy and excitation dynamics of condensed molecular systems*, chp. 3, North-Holland publishing company (1983), pp. 129-135.
  - <sup>6</sup> Morrel H. Cohen and J. Ruvalds, *Phys. Rev. Lett.* **23**, 1378 (1969).
  - <sup>7</sup> R. Tubino and J. L. Birman, *Phys. Rev. Lett.* **35**, 670 (1975).
  - <sup>8</sup> R.S. Mackay, *Physica A* **288**, 174 (2000).
  - <sup>9</sup> V. Hizhnyakov, D. Nevedrov and A. J. Sievers , *Physica B* **316-317**, 132 (2002).
  - <sup>10</sup> J. Dorignac and S. Flach, *Phys. Rev. B* **65**, 214305 (2002).
  - <sup>11</sup> V. Fleurov, *Chaos* **13**, 676 (2003).
  - <sup>12</sup> A. J. Sievers and S. Takeno, *Phys. Rev. Lett.* **61**, 970 (1988); S. Takeno, K. Kisoda and A. J. Sievers, *Progress of Theoretical Physics Supplement* **94**, 242 (1988).
  - <sup>13</sup> R.S. MacKay and S. Aubry, *Nonlinearity* **7**, 1623 (1994).
  - <sup>14</sup> L.D. Landau and E. M. Lifshits, *Quantum Mechanics (Non-Relativistic Theory)*, Pergamon Press, New York (1965).
  - <sup>15</sup> William H. Press, *Numerical Recipes in Fortran*, Cambridge University Press (1992), pp. 462-475 ; <http://www.nr.com/> .

<sup>16</sup> H. Mao and R.J. Hemley, *Rev. Mod. Phys.* **66**, 671 (1994).

<sup>17</sup> O. A. Dubovskii, A. V. Orlov and V. A. Semenov, *Physics of the Solid State* **45**, 326 (2003).

Table caption

Tab. I: Values of the coefficient  $2 \langle \phi_{\alpha_i} | X_i | \phi_{0_i} \rangle^2$  for the different nonlinear coefficients  $A_3$  and  $A_4$  of the onsite potential that are used for the computations of Figs. 5-11.

### Figure captions

Fig. 1: Energy spectrum of the Hamiltonian of a single *He* atom embedded into a double-well potential (plotted into the insert). The maximum rises to  $E_0 = 0.1eV$  and the minima are separated by  $b = 2\text{\AA}$ : (a) The semi-classical calculation (square symbols, dashed line) is compared to the diagonalization (circle symbols, solid line) onto the truncated Einstein basis with a frequency  $\omega_0 = \sqrt{32.E_0/(ma_0^2)}$ ; (b) The later method converges when the basis cutoff  $N$  increases and it becomes exact when  $N$  is large enough.

Fig. 2: Plot of the bracket  $\langle \phi_{\alpha,i} | X_i | \phi_{0,i} \rangle$  of the displacement at site  $i$  for the nonlinear parameters  $A_4 = 0.2$  and  $A_3 = 0$  (solid line with triangle symbols) and  $A_4 = 0.01$  and  $A_3 = 0.13$  (dashed line with circle symbols)

Fig. 3: (color online) For a unitless coupling  $C = 0.1$ , comparison between the exact eigenvalue calculation (dark solid line) and the onsite state product Bloch waves method (see in the text Sec. II) for the Hamiltonian of a 1D chain of  $S = 25$  harmonic oscillators. The spectrum is arranged in increasing order and it is measured with respect to the groundstate. The computation is performed for different upper number of onsite excitations  $N_{oe} = 4$  (blue solid line with circle symbols),  $N_{oe} = 3$  (red dotted line with squares) and  $N_{oe} = 2$  (green dot-dashed line with triangles). The precision increases with  $N_{oe}$ .

Fig. 4: Comparison between the results of Ref. 2 (diamond symbols) and the onsite state product waves method (for further details see Sec. II) (circle symbols), for a 4-site chain of quantum quartic oscillators.

Fig. 5: Plots of the low energy branches of the energy spectrum of a 1D chain of  $S = 33$  atoms length, for  $C = 0.05$ ,  $A_3 = 0$ ,  $A_4 = 0.2$  (a) and  $A_4 = 0.02$  (b). The left insert shows a magnification of the fundamental branch while the overtone region is magnified in the right insert. The biphonon branch is marked by  $\{\{2\}\}$  and the free two-phonon bands by  $\{\{11\}\}$ . The same tags point into the insert. The Y-axis unit is  $\hbar\Omega$  and its zero is the groundstate.

Fig. 6: Same as Fig. 5 but for different parameters, i.e.,  $A_4 = 0.01, A_3 = 0.13$  (a) and

$A_3 = 0.105$  (b). The Y-axis unit is  $\hbar\Omega$ .

Fig. ??: Versus the unitless coupling  $C$ , plot of the energy spectrum of a quantum 1D chain of  $S = 19$  atoms for  $A_4 = 0.2, A_3 = 0$ . (a), for  $A_4 = 0.01, A_3 = 0.13$  (b). The tags are explained in the text.

Fig. 7: (color online) On the left hand side, energy spectra of the two dimensional square lattices in the region of the first overtone for  $C = 0.025, A_3 = 0$  and  $A_4 = 0.1$  (top) and for same parameters but  $A_4 = 0.025$  (bottom). The lattice size is  $S = 13 \times 13$  atoms. On the right hand side, profiles of the left-hand side spectra along the direction  $[11]$ . The inserts show the magnification of the phonon branch and the biphonon energy region.

Fig. 8: (color online) Versus the unitless distance  $n$ , plot of the correlation functions  $f_\Phi(n)$  for 3 eigenstates of  $H$  (one-dimensional network with  $S = 23$ ) and for parameters  $A_4 = 0.2, A_3 = 0, C = 0.05$ . The eigenstates correspond to the phonon states (a), the biphonon (b) and the tri-phonon (c) with for each of them different wave vectors  $q = 0$  (circles),  $q = 4\pi/S$  (triangles),  $q = 8\pi/S$  (diamonds),  $q = 12\pi/S$  (squares) and  $q = 16\pi/S$  (triangles). The inserts in Fig. (b) and (c) show the magnifications of the zero y-axis of the corresponding figures.

Fig.9: (color online) Versus the unitless distance  $n$ , plot of the correlation functions  $f_\Phi(n)$  for 3 eigenstates of  $H$  (one-dimensional network with  $S = 23$  atoms) for parameters  $A_4 = 0.01, A_3 = 0.13, C = 0.05$ . The eigenstates correspond to the phonon states (a), the biphonon (b) and the triphonon (c) with same wave vectors as in Fig. 8. The inserts in Fig. (b) and (c) show the magnifications of the zero y-axis of the corresponding figures.

Fig. 10: (color online) Versus the unitless distance  $n$ , plot of the correlation functions  $f_\Phi(n)$  for two eigenstates of  $H$  and for parameters  $A_4 = 0.02, A_3 = 0., C = 0.05$ . The eigenstates correspond to the phonon states (a) and the biphonon (b) with same wave vectors as in Fig. 8. The insert in Fig. (b) shows a magnification of the zero y-axis

Fig. 11: (color online) Same as Fig. 10 for parameters  $A_4 = 0.01, A_3 = 0.105, C = 0.05$ .

The insert in Fig. (b) shows a magnification of the zero y-axis

$2 \langle \phi_{\alpha_i}   X_i   \phi_{0_i} \rangle^2$	$A_4 = 0.2 \ A_3 = 0$ Fig.5(a) & Fig.8	$A_4 = 0.01 \ A_3 = 0.13$ Fig.6(a) & Fig.9	$A_4 = 0.02 \ A_3 = 0$ Fig.5(b) & Fig.10	$A_4 = 0.01 \ A_3 = 0.105$ Fig.6(b) & Fig.11
$\alpha = 1$	0.74	1.06	0.95	1.03
$\alpha = 2$	0.	$2.9710^{-2}$	0.	$1.1610^{-2}$
$\alpha = 3$	$7.3910^{-4}$	$2.3610^{-3}$	$7.910^{-5}$	$3.310^{-4}$
$\alpha = 4$	0.	$3.9110^{-4}$	0.	$1.0910^{-5}$
$\alpha = 5$	$8.4510^{-7}$	$5.4510^{-5}$	$1.4510^{-8}$	$4.3910^{-7}$

TABLE I: (2004) L. Proville

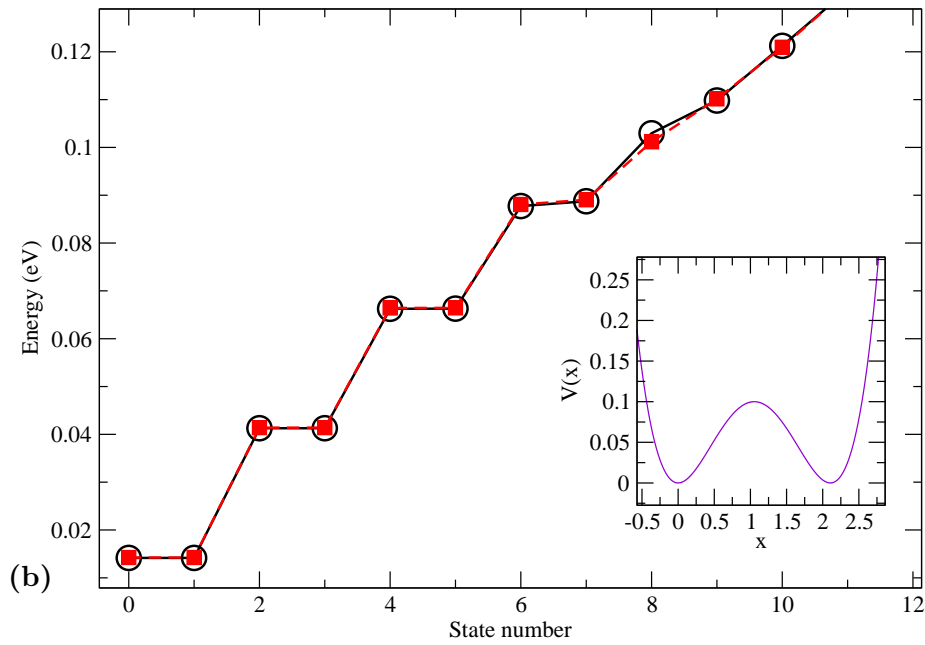
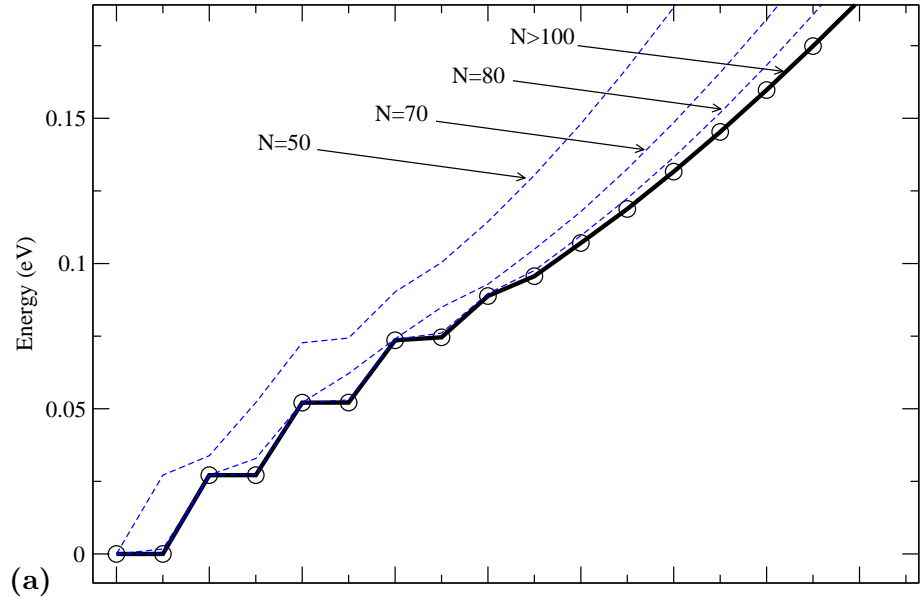


FIG. 1: (2004) L. Proville

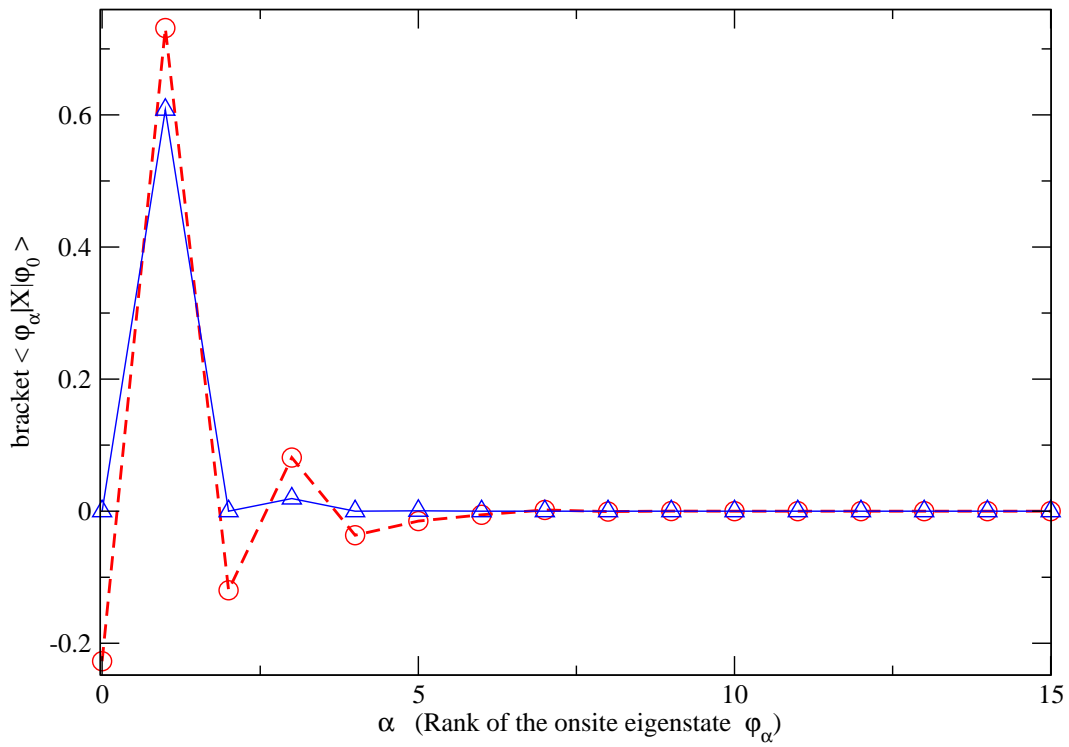


FIG. 2: (2004) L. Proville

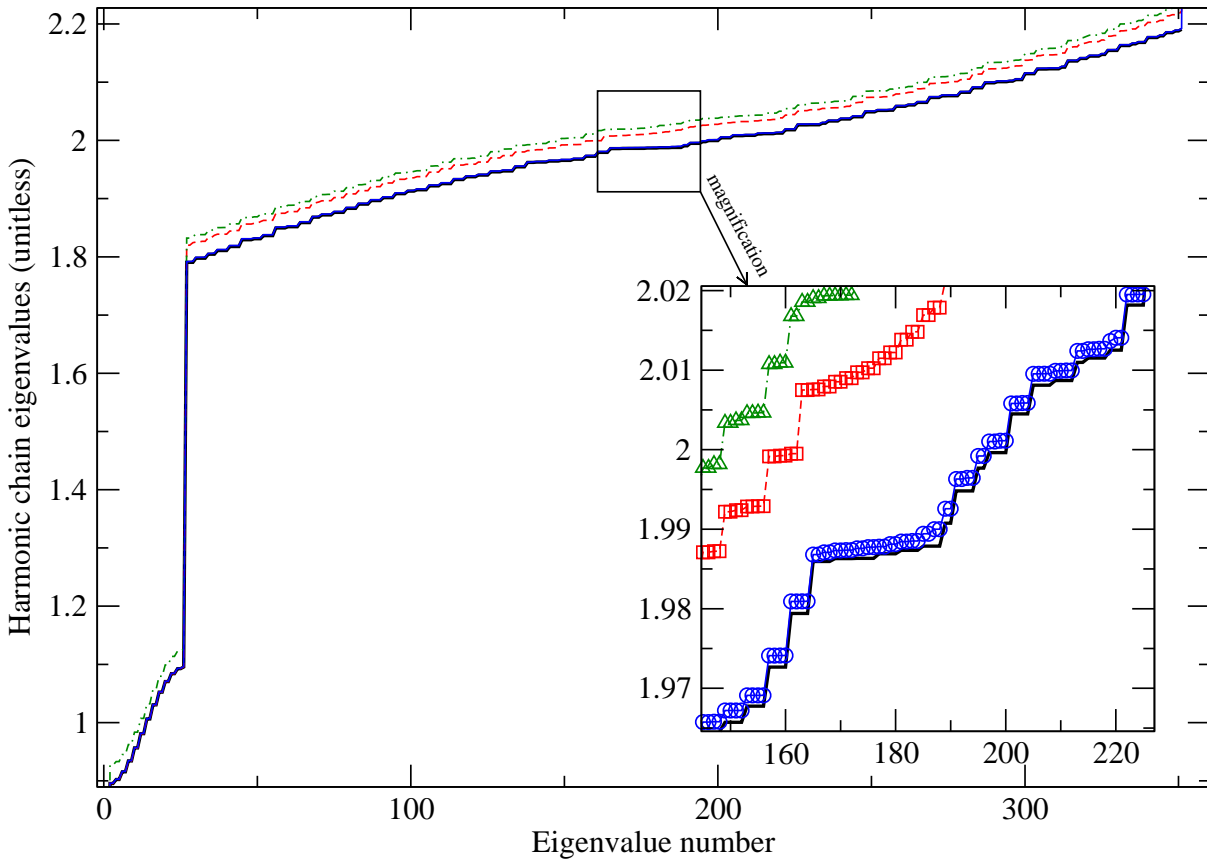


FIG. 3: (2004) L. Proville

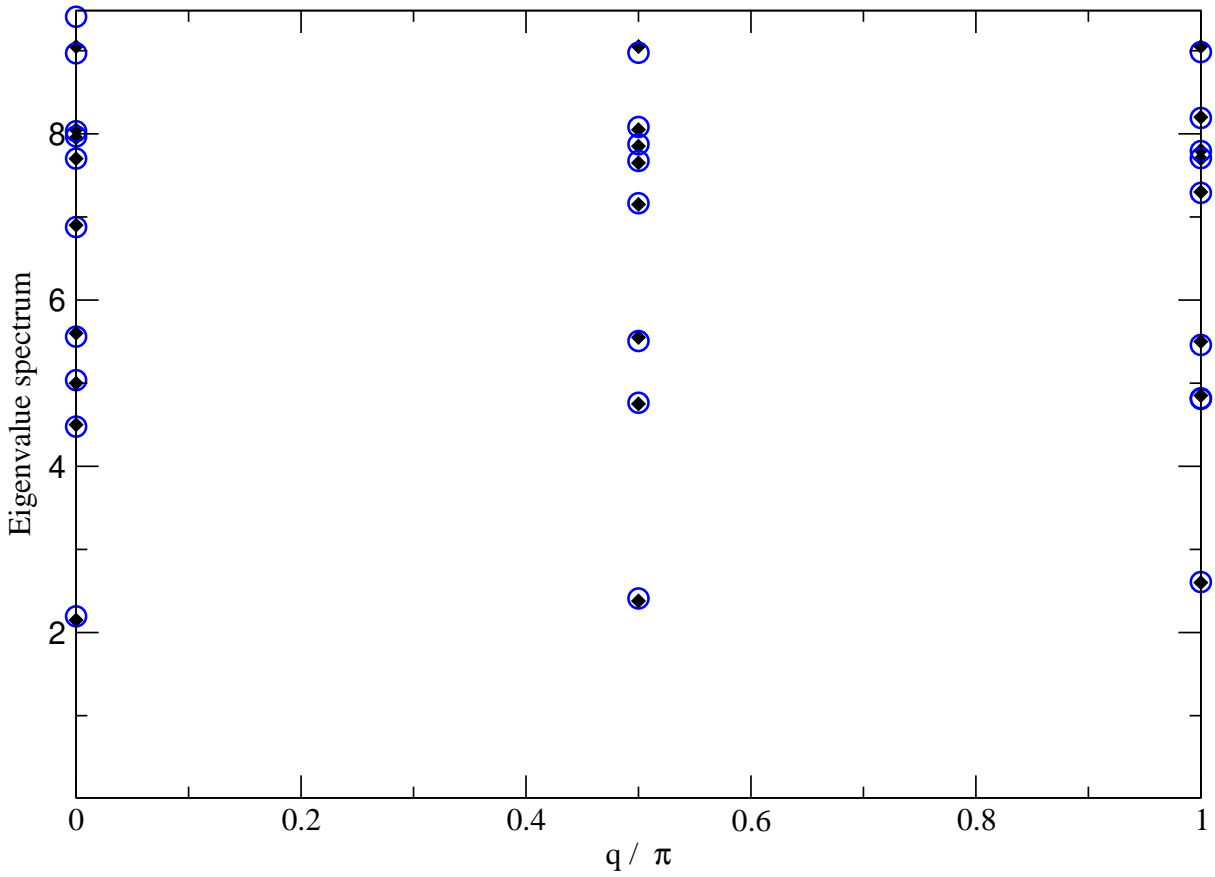


FIG. 4: (2004) L. Proville

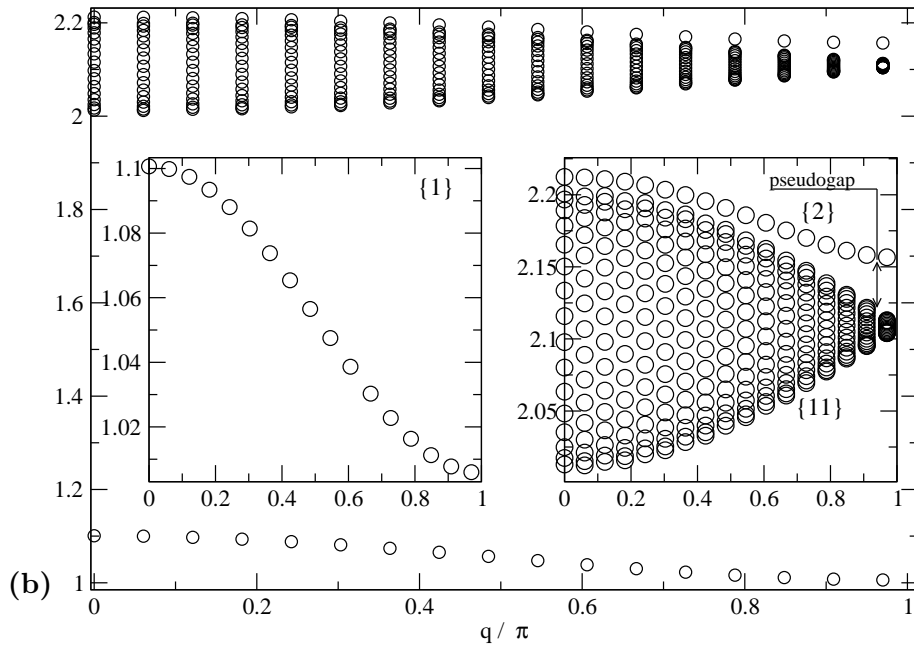
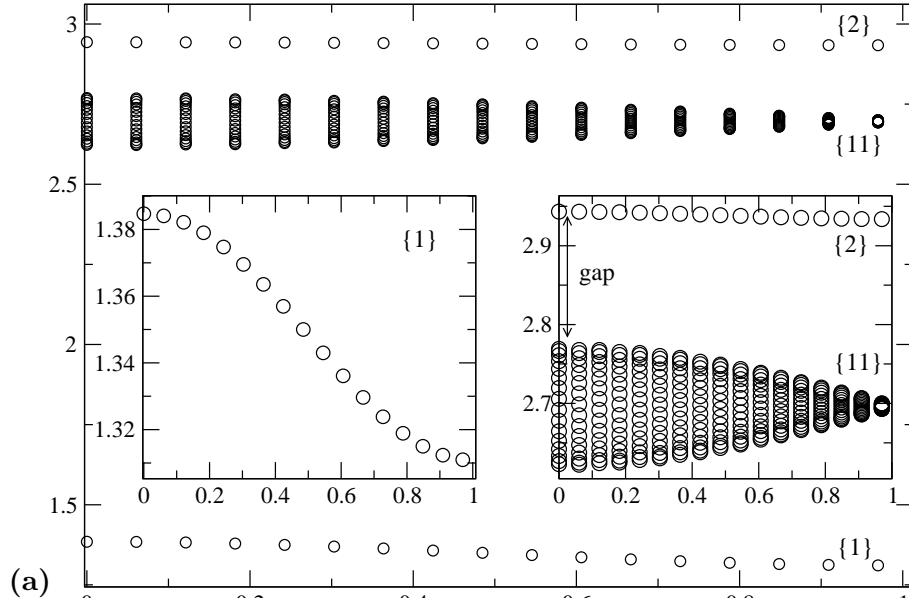


FIG. 5: (2004) L. Proville

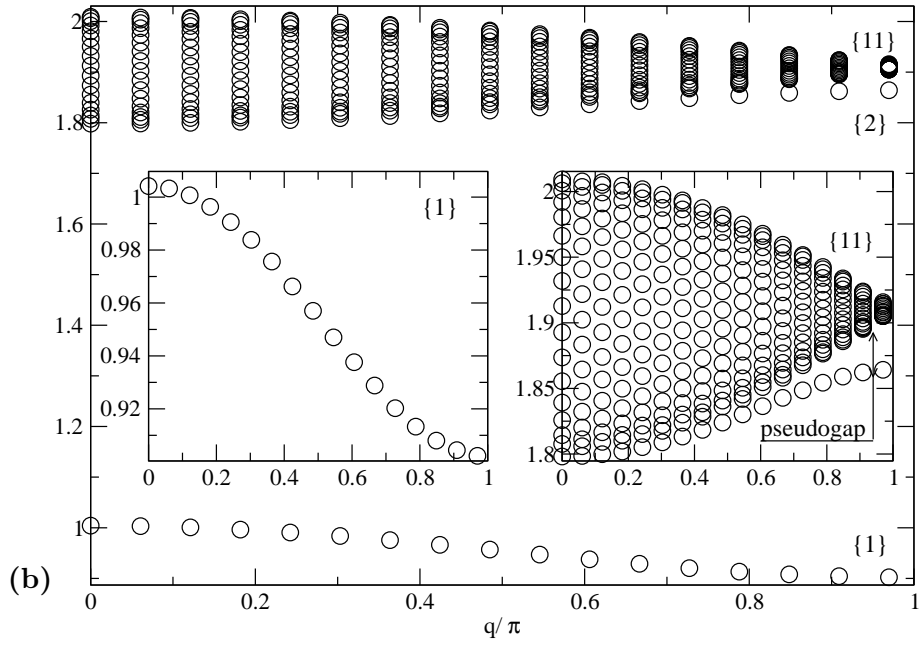
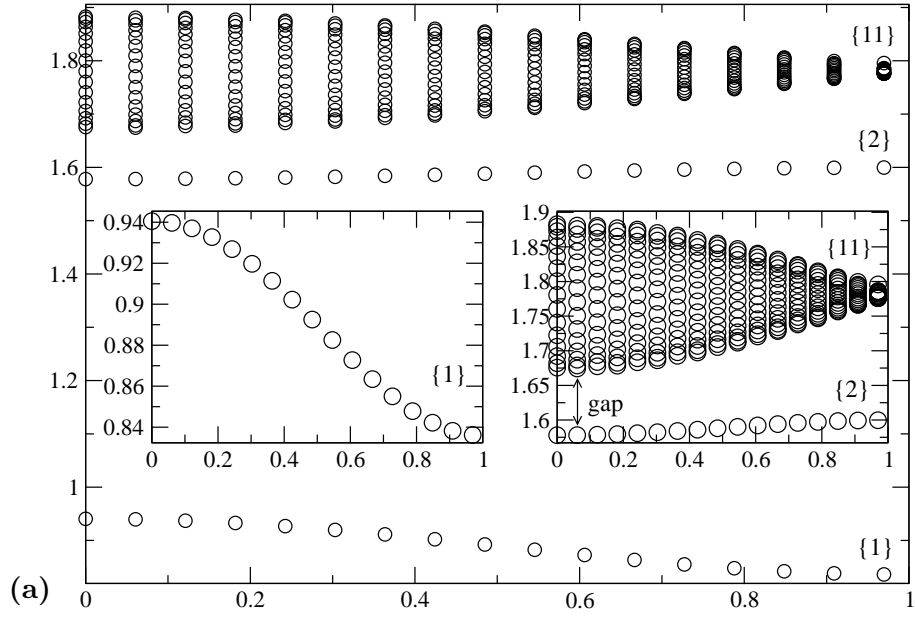


FIG. 6: (2004) L. Proville

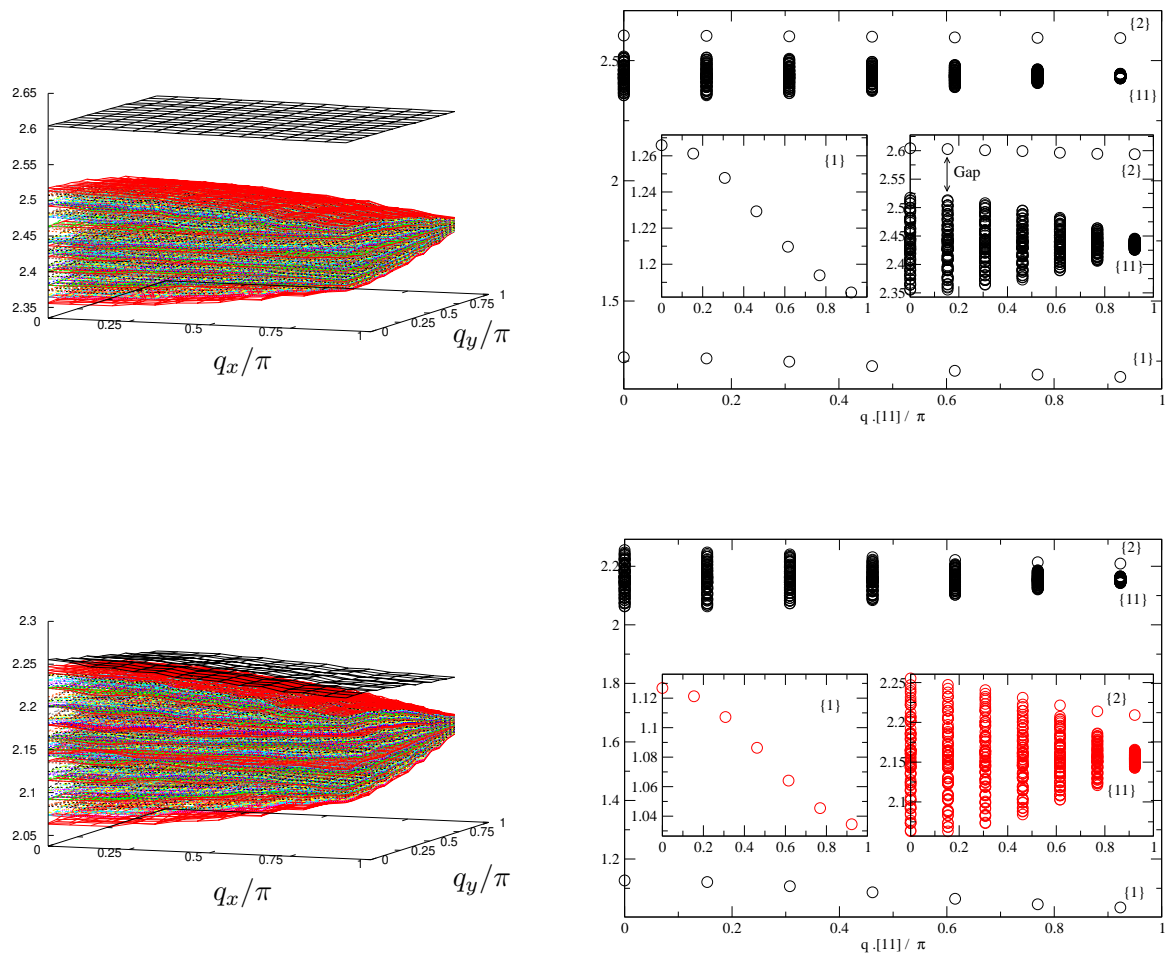


FIG. 7: (2004) L. Proville

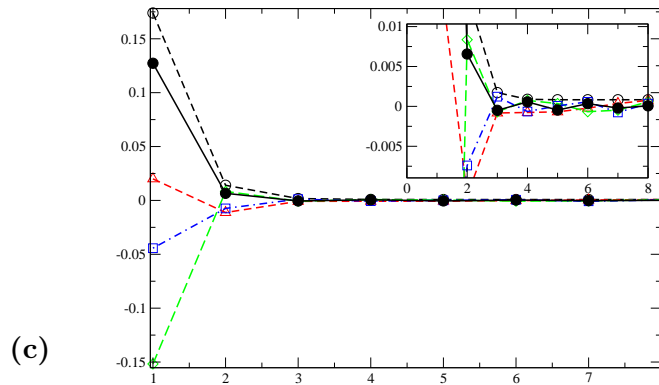
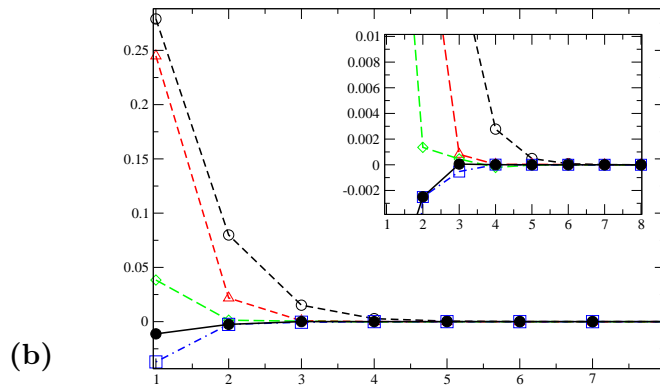
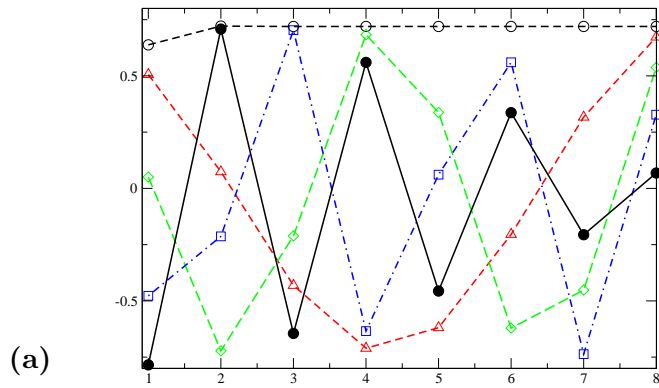


FIG. 8: (2004) L. Proville

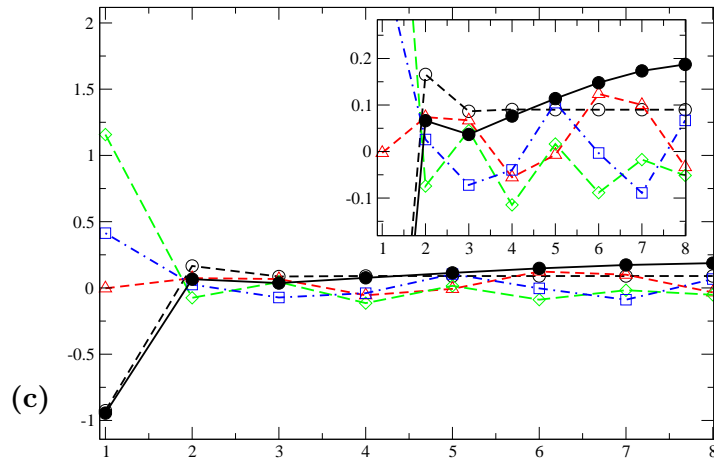
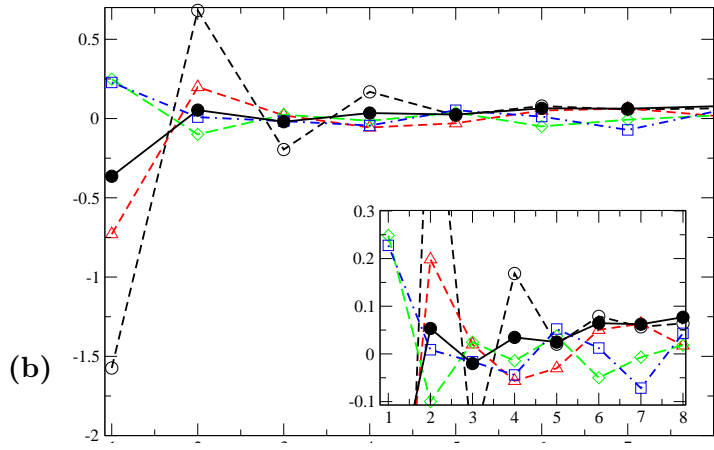
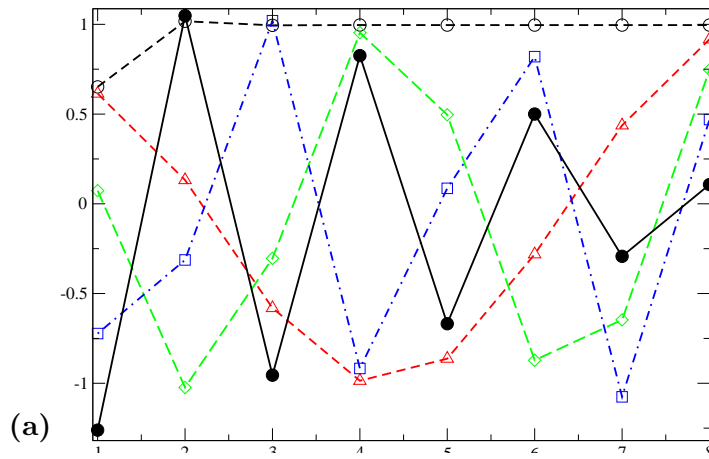


FIG. 9: (2004) L. Proville

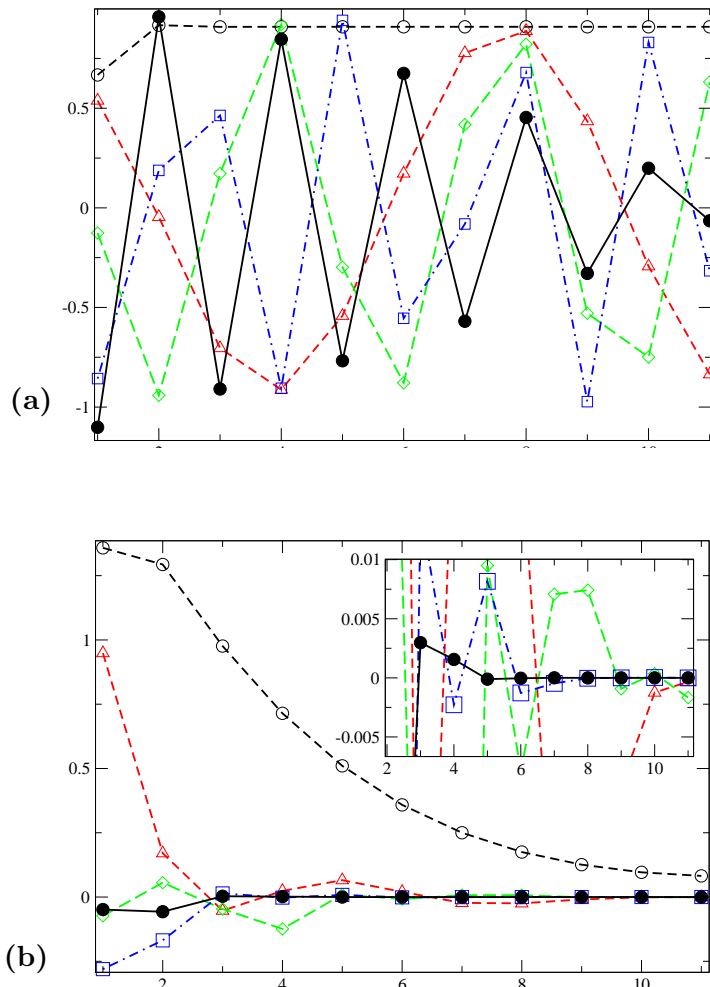


FIG. 10: (2004) L. Proville

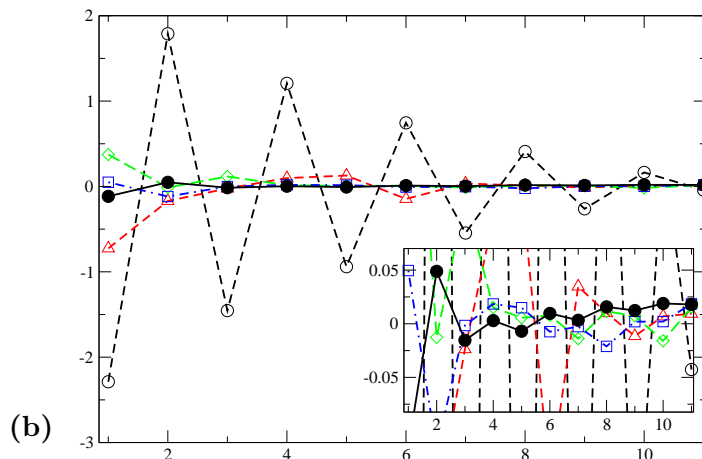
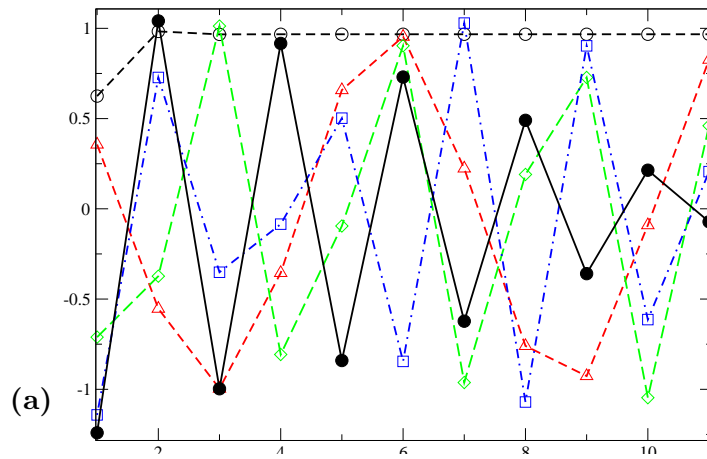


FIG. 11: (2004) L. Proville

This figure "fig7aPROVILLE.png" is available in "png" format from:

<http://arxiv.org/ps/cond-mat/0403516v1>

This figure "fig7bPROVILLE.png" is available in "png" format from:

<http://arxiv.org/ps/cond-mat/0403516v1>